Title: Semi-automated protocol to quantify and characterize fluorescent three-dimensional vascular images

Danny F. Xie[1,2], Christian Crouzet[1,2], Krystal LoPresti[1,2], Yuke Wang[1,2], Christopher Robinson[1,2], William Jones[1], Fjolla Muqolli[1], Chuo Fang[3], David H. Cribbs[4], Mark Fisher[1,3,4,5], and Bernard Choi[1,2]

Affiliations:

[1]Beckman Laser Institute and Medical Clinic, University of California-Irvine, Irvine, CA, USA

[2]Department of Biomedical Engineering, University of California-Irvine, Irvine, CA, USA

[3]Department of Neurology, University of California-Irvine, Irvine, CA, USA

[4]Institute for Memory Impairments and Neurological Disorders, University of California-Irvine, Irvine, CA, USA

[5]Department of Pathology & Laboratory Medicine, University of California-Irvine, Irvine, CA, USA

Abstract

The microvasculature facilitates gas exchange, provides nutrients to cells, and regulates blood flow in response to stimuli. Vascular abnormalities are an indicator of pathology for various conditions, such as compromised vessel integrity in small vessel disease and angiogenesis in tumors. Traditional immunohistochemistry enables visualization of tissue cross-sections containing exogenously labeled vasculature. Although this approach can be utilized to quantify vascular changes within small fields-of-view, it is not a practical way to study the vasculature on the scale of whole organs. Three-dimensional (3D) imaging presents a more appropriate method to visualize the vascular architecture in tissue. Here we describe the

complete protocol that we use to characterize the vasculature of different organs in mice encompassing the methods to fluorescently label vessels, optically clear tissue, collect 3D vascular images, and quantify these vascular images with a semi-automated approach. To validate the automated segmentation of vascular images, one user manually segmented fifty random regions of interest across different vascular images. The automated segmentation results had an average sensitivity of 80±8% and an average specificity of 90±5% when compared to manual segmentation. Applying this procedure of image analysis presents a method to reliably quantify and characterize vascular networks in a timely fashion. This procedure is also applicable to other methods of tissue clearing and vascular labels that generate 3D images of microvasculature.

Introduction

The microvasculature facilitates gas exchange, provides nutrients to cells, and regulates blood flow in response to stimuli. Thus, it plays a fundamental role in the survival and health of tissues and organs. Vascular abnormalities are an indicator of pathology for various conditions, such as compromised vessel integrity in small vessel disease and angiogenesis in tumors (1,2). In addition, impaired blood flow to the brain is associated with neurodegenerative diseases such as Alzheimer's disease (3).

Traditional immunohistochemistry enables visualization of tissue cross-sections containing exogenously labeled vasculature. Although this approach can be used to quantify vascular changes within small fields-of-view, it is not a practical way to study the vasculature on the scale of whole organs. Furthermore, traditional immunohistochemistry requires the sectioning of tissue into thin (6-40 μm) sections, which effectively limits visualization of features to planar views and thus impedes facile 3D visualization of vascular architecture.

Volumetric imaging of tissue samples is vital to studying the microvasculature in its

native state. The main limitation to 3D imaging of tissue samples is optical scattering resulting from the microscopic variations of refractive index occurring in most biological tissues. Organic solvents and aqueous solvents have been used to reduce tissue turbidity by achieving refractive index matching (4,5). CLARITY is a popular method used for tissue clearing that involves embedding of the sample into a hydrogel and using an electric current to remove lipids from the sample (6). Other tissue clearing procedures have advantages and disadvantages associated with clearing time, extent of clearing, and preservation of original tissue characteristics (size, endogenous fluorescence, etc.).

Quantitative analysis of microvasculature is essential to understand how structural variations in the microvascular network may change for different pathological states (7). The feasibility of such analysis depends on accurate, ideally automated segmentation methods for isolating the microvasculature from the background due to the hundreds of gigabytes of data generated with high-resolution 3D imaging. Various groups have developed automated algorithms to perform quantitative characterization of vascular images (8,9). Each method varies in complexity, processing time, and computational requirements.

We currently use iDISCO (immunolabeling-enabled three-dimensional imaging of solvent-cleared organs) as our primary method of tissue clearing (4,10). Briefly, iDISCO consists of methanol dehydration, lipid removal with dichloromethane, and refractive index matching with dibenzyl ether. iDISCO is a fast, simple-to-implement clearing method that enables deep-tissue imaging. It is compatible with many exogenous labels often used for traditional immunohistochemistry. We previously demonstrated the effectiveness of iDISCO in combination with lectin-DyLight-649 for 3D visualization of vasculature in a mouse brain (10). We also have used Prussian blue labelling of hemosiderin (11–13), a by-product of cerebral microhemorrhages, with iDISCO-cleared brains and lectin-DyLight-649 labelling.

In this paper, we first review different methods for vascular labeling in conjunction with optical clearing that have been published by other groups. Next, we describe the complete

protocol that we use for imaging the vasculature in different organs in mice. Specifically, we report on sample collection and perfusion of lectin-DyLight-649 followed by application of additional labels as desired and optical clearing. We then describe our procedure to obtain 3D confocal microscopy images. Finally, we describe our semi-automated approach to process the resulting images and quantify the vascular architecture in three dimensions.

Vascular imaging with various vessel labels and optical clearing techniques

Through reviewing the literature on 3D vascular imaging of cleared tissue, one will quickly realize the large variability in methodology across different experiments (see Table 1 for specific references). For example, blood vessels can be visualized with transgenic animals expressing a fluorescent protein in endothelial cells, labeled *in vivo* with intravascular dyes, or labeled *ex vivo* with immersion-based antibody labelling. In addition, tissue preparation can vary from thick tissue sections and whole organs to whole-mount specimens, depending on the purpose of an experiment. Finally, clearing procedures can be grouped into aqueous solvents (14–19), organic solvents, and hydrogel-based.

When selecting a clearing procedure, it is essential to consider its compatibility with the chosen vascular label. Endogenous fluorescence intensity is known to be reduced when using the iDISCO protocol; hence, an alternative vascular label would be preferred. Imaging of cleared samples is typically performed with confocal microscopy or light-sheet microscopy. Lastly, vascular-related metrics, such as vessel diameters and vessel density, are quantified with existing software such as FIJI and Imaris, or custom-designed software such as ClearMap 2.0.

We have reviewed several optical clearing methods utilized to image vasculature. They are organized in Table 1 by clearing method, tissue type, vessel label, and quantification. Vascular images in cleared tissue from select publications are included in Fig 1B-D. FDISCO is

an organic solvent-based clearing method derived from the 3DISCO method. In developing FDISCO, Qi *et al.* found that they could achieve superior fluorescent signals of CD31-labelled vessels by optimizing temperature and pH conditions (Fig 1B, 1B') (20,21). Moy *et al*. visualized vessels with an intravascular fluorescent dye along with FocusClear (Figure 1C, 1C') (8). They were able to quantify functional vascular density in different regions of cardiac tissue with a custom MATLAB algorithm (21). With a polyethylene glycol-associated solvent system (PEGASOS), researchers developed a clearing technique that preserved both hard and soft tissue structures (Fig 1D, 1D') (22), allowing for vascular imaging throughout an entire specimen.

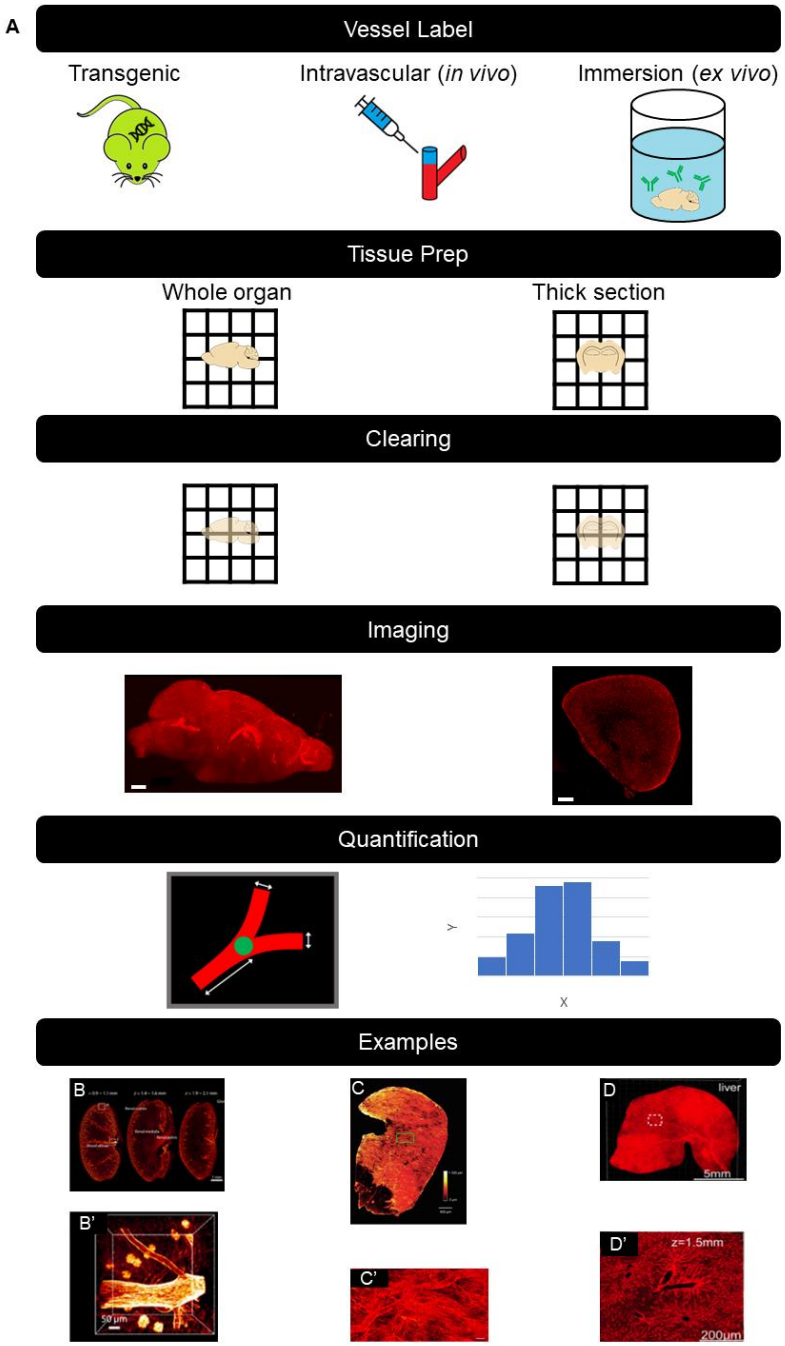

Fig 1. A) Illustrations of the critical steps and workflow for vascular visualization in cleared tissue. B-D) Examples of vascular visualization in literature. B) Visualization of CD31-labeled mouse kidney vasculature with FDISCO (20). B') Magnified view of 1B. C) Visualization of DiI-labeled mouse heart vasculature with FocusClear (8). C') Magnified view of 1C. D) Visualization of liver vasculature from *Tie2-Cre* mouse model with PEGASOS (22). D') Magnified view of 1D).

Table 1. Summary of different approaches to visualize 3D microvasculature in optically cleared tissues.

Clearing agent(s)	Organ(s)	Vascular label	Quantification Method/Tool	Quantified Metrics
MACS (14)	brain, heart, lung, spleen, femur, kidney, spinal cord, embryo, entire body	DiI, tetramethylrhodamine-conjugated dextran	Custom algorithm via Python, Imaris: surface function	glomerulus number and glomerulus volume; general metrics (imaging depth, size change, fluorescence intensity)
SeeDB, SeeDB2, 3DISCO, uDISCO, iDISCO, CUBIC, simplified CLARITY method, 75% v/v glycerol, Ce3D, FRUIT (23)	lymph nodes	CD31	Imaris: surface function, ImageJ	general metrics (imaging depth, size change, fluorescence intensity)
sodium dodecyl sulfate/sodium deoxycholate with Sca*l*eCUBIC-2 (24)	brain	RITC-Dex-GMA, Texas red lectin, CD31, αSMA	N/A	capillary diameters, signal-to-noise ratio
iDISCO (4)	brain, peripheral nervous system, kidney, muscle, heart, whisker pad, entire embryo	PeCAM	N/A	N/A
iDISCO with CUBIC (25)	ovary	endomucin	N/A	N/A
FDISCO (20)	brain, kidney	AlexaFluor647, CD31, lectin-DyLight-649	Imaris, ImageJ	general metrics (size change, imaging depth, fluorescence quantification)
Sca*l*eS (15)	brain	Texas Red lectin	custom C++, commercial Volocity, commercial Igor Pro	microglia and Aβ plaques with custom C++, distance between microglia and Aβ plaques
3DISCO (26)	brain	FITC albumin-gelatin hydrogel	Imaris, ImageJ	vessel density, vessel diameter
thiazone with PEG-400 (27)	dorsal skin	N/A (imaged blood flow via LSI)	N/A	bloodflow via LSCI
iDISCO (28)	brain	Dye-conjugated secondary antibodies	ClearMap	Aβ deposits

CLARITY, TDE (29)	brain	lectin-FITC, gel-BSA-FITC, gel-BSA-TRITC	Markov random field based algorithm, ImageJ, Amira 5.3 software	automatic segmentation, vessel diameter, vessel length
FACT (30)	brain, spinal cord, heart, lung, adrenal gland, pancreas, liver, esophagus, duodenum, jejunum, ileum, muscle, bladder, ovary, uterus	CD31, auto fluorescence	Imaris	segmentation
CUBIC, BABB (16)	heart	FITC-lectin, 649-lectin, CD31	N/A	N/A
BABB (31)	heart	PECAM1	N/A	N/A
DBE, SCALE, CLARITY, CUBIC (32)	heart and embryo	GFP		
vDISCO (33)	whole mouse	GFP, lectin	ImageJ, ClearMap	signal level, microglia distribution
3DISCO (34)	brain	tomato lectin	N/A	N/A
CLARITY (35)	brain	fluorescein-conjugated tomato lectin	Amira	area, volume, perimeter, and length of stained vessel
CLARITY with ScaleA2 (36)	ovary, uterus, lung, liver	tdTomato	Ilastik, Imaris	segmentation, total vessel length, vessel mean diameter, vessel straightness, total number of branching points
PEGASOS (22)	whole mouse	αSMA, GS-IB4 isolectin dye, collagen IV	Imaris	vessel density
iDISCO (9)	brain	CD31, podocalyxin, collagen IV, smooth muscle actin, transgelin, von Willebrand factor	ClearMap 2.0, TubeMap	vascular density, vascular orgnaization, vascular remodeling
ethyl-cinnamate (37)	liver, skin, lung, heart, muscles, pancreas, brain, kidney	In-house developed NIR fluorescent dye (MHI148-PEI)	Leica LAS X	segmentation, volume of glomerulus
X-CLARITY (38)	placenta	DiI	Imaris, Image-Pro Premier	N/A

CLARITY, iDISCO (39)	brain	lectin-DyLight, lectin-FITC, anti-CD31	Imaris, segmentation	number of branches, total vessel length, total vessel volume, total vessel area, diameter of single segments per volume, distance between cells and nearest vessel
PEGASOS (40)	bone, teeth	tdTomato	Imaris	blood vessel volume
Sca*l*eS (17)	pancreas	lectin-DyLight	N/A	N/A
CLARITY (41)	retina	Griffonia lectin	Angiotool, ImageJ, Vaa3D, MATLAB, APP-2.0	network tracing, vessel percentage area, total number of junctions, junction density, total vessel length, average vessel length, total number of endpoints, mean lacunarity
No clearing approach (42)	retina, heart	DiI	N/A	N/A
FocusClear (18)	small intestine	DiI	N/A	N/A
FocusClear, ScaleSQ, RIMS, sRIMS (19)	brain	Lectin-Dylight649	MATLAB	optical properties, vascular density
FRUIT 100 (43)	brain tumor	DiI	N/A	N/A
FocusClear (44)	brain	DiI	N/A	optical properties
FocusClear (45)	brain	DiI	MATLAB	functional vascular density

Three-dimensional quantitative analysis of microvasculature imaged in thick tissue sections

Microvascular labeling is performed with an injection of a lectin conjugated to a fluorophore. In our work, we have focused on the DyLight-649 fluorophore. As the lectin travels through the circulatory system, it binds to glycoproteins adjacent to endothelial cells of the vascular wall. This binding allows for labeling of the vascular network within every organ of the body.

An overview of our workflow is outlined below in Fig 2. We administer lectin-DyLight-649 via retroorbital injection. The lectin is allowed to circulate throughout the body prior to cardiac perfusion with saline followed by formalin. Mouse brains are then extracted, bisected into hemispheres, and sectioned into thick (0.5-1.0mm) sections. Each section is then imaged using confocal microscopy to generate image stacks of the complete section throughout its entire thickness. Segmentation is performed by a custom MATLAB (MathWorks, Natick, MA) script. Finally, neuTube, an open-source neuron tracing software, is used to extract diameter measurements of the vessel structures (46). Below, we describe in detail the materials and methods we use.

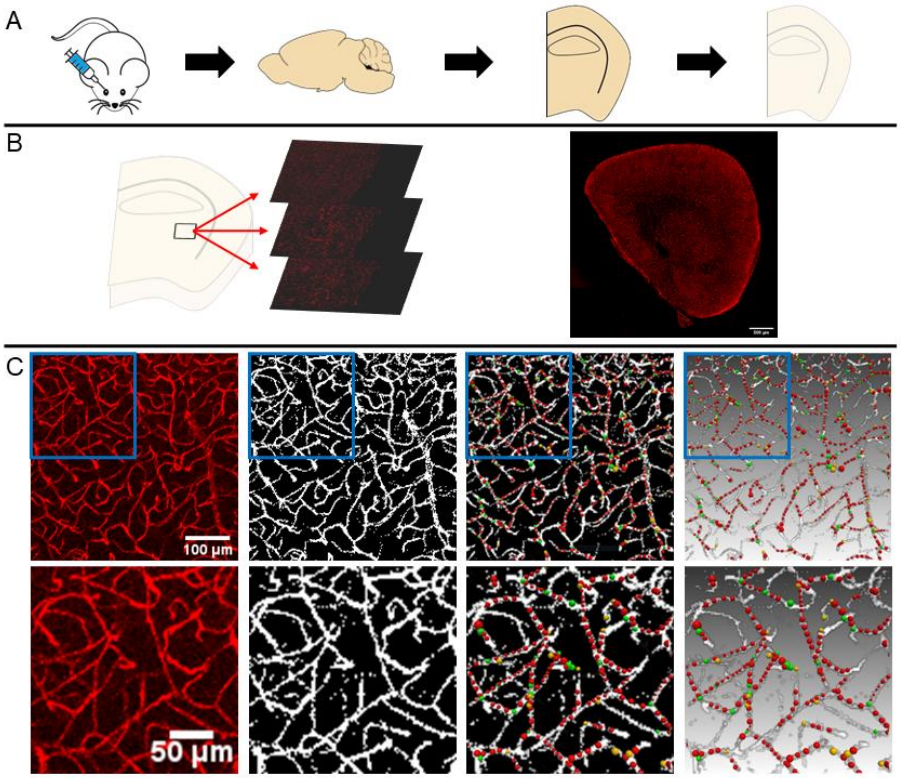

Fig 2. Workflow for 3D visualization and quantitation of microvasculature in thick tissue sections. A) Vasculature is labeled via retroorbital injection of lectin-DyLight-649. Brains are then sectioned and cleared. B) Depiction of z-stack imaging and tile stitching to visualize an entire sample in 3D via confocal microscopy. C) From left to right: representative example of a raw image of the vasculature, segmented vasculature via MATLAB, and traced vasculature via neuTube.

Methods

Equipment and supplies

Reagents:

- Saline solution (Aspen Veterinary Resources, NDC No. 46066-807-50)
- 10% formalin solution (Sigma-Aldrich Product Code HT50-1-1)
- PBS with 0.02% sodium azide solution (Syringa Lab Supplies, Part No. 11001)
- Potassium ferrocyanide (Sigma: P3289-500G)
- Hydrochloric acid (Fisher: A144-212)
- Methanol (Fisher: A412S)
- Deionized water
- Dichloromethane (Sigma: 270997-100ML)

- Dibenzyl ether (Sigma: 108014-1KG)

Equipment:

- 2x 10 mL syringes (Sigma-Aldrich: Z683604)
- 1x 23G x ¾ x 12" butterfly needle (Vaculet, 26766)
- 3x hemostat clamps (Excelta: 37SE)
- 1x bone scissors (Fine Science Tools: 91604-09)
- 1x forceps (Fine Science Tools: 11000-12)
- 1x scissors (Excelta: 290)
- 1x angled scissors (Fine Science Tools: 15010-10)
- 1x spatula (Fine Science Tools: 10089-11)
- 1x syringe pump (Harvard Apparatus Model 11 Plus)
- 1x 20 mL glass scintillation vial (Grainger: 3LDT2)
- Aluminum foil
- Tape
- Liquid absorbent mats
- Isoflurane chamber (E-Z Systems: EZ-178)
- Nose cone (E-Z Systems: EZ-103A)
- Magnetic stir plate with stir bar (Corning PC 353 Stirrer)
- Orbital shaker (Scilogex: SK-D1807-E)
- Scale
- Weigh boats
- Pipette controller (Grainger: 49WF85)
- Serological pipette tips
- 1.5 mL opaque microcentrifuge tube (Argos Technologies: 06333-80)
- Microcentrifuge tube rack
- Pipettes
- 18-gauge needle
- Leica TCS SP8 microscope

Software:

- MATLAB (https://www.mathworks.com/)
- FIJI (https://imagej.net/Fiji)
- neuTube (https://www.neutracing.com/)

Reagent setup:

- *10% potassium ferrocyanide (PF) solution*
  - Dissolve the appropriate amount of PF in deionized water (DIW) (10 g of PF per 100 mL of DIW) to create a 10% PF solution. Use a magnetic stir bar and magnetic stir plate to dissolve potassium ferrocyanide.
- *20% hydrochloric acid (HCl) solution*
  - Dilute the appropriate amount of stock HCl solution in DIW (20 mL of stock HCl per 80 mL of DIW) to create 20% HCl solution. Perform this step under a fume hood.
- *Potassium ferrocyanide/hydrochloric acid working solution*
  - Mix 1 part 10% potassium ferrocyanide solution per 1 part 20% HCl solution

Cardiac perfusion protocol and sample preparation

Cardiac perfusion

Begin by anesthetizing a mouse using an isoflurane chamber with 1.5 L/min of oxygen and 4.0% isoflurane. Once the mouse is anesthetized, remove it from the chamber and place its snout in a nose cone at 1.5 L/min oxygen and 1.5% isoflurane. Administer a solution of lectin-DyLight-649 (200 µL, 25% lectin-DyLight and 75% saline) via retroorbital injection (see Fig 3A,B) (47,48). Allow the solution to circulate for about 20 minutes before proceeding with the cardiac perfusion (49).

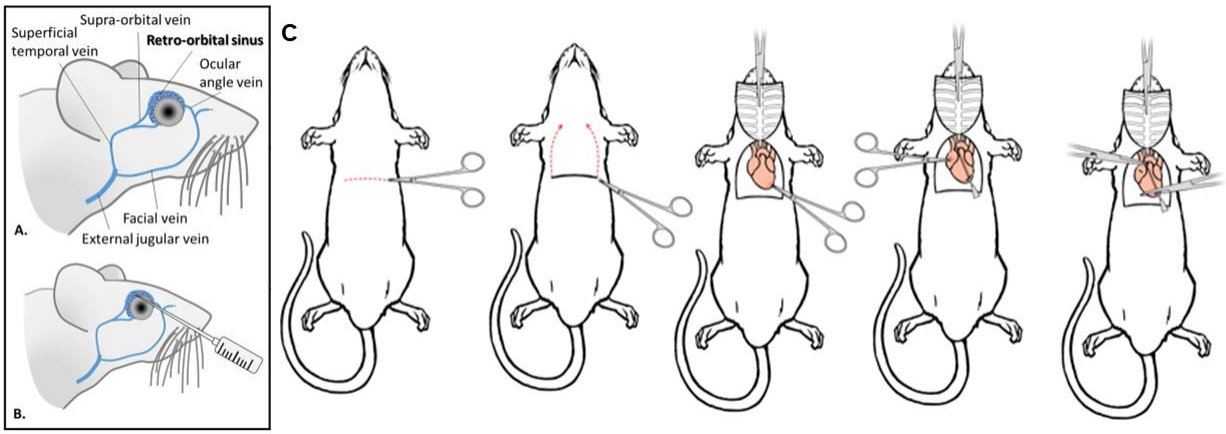

Fig 3. Key steps for animal procedures. A,B) Retroorbital injection diagram. Correct needle placement is shown. C) Incision points for opening the chest cavity. A lateral incision beneath the diaphragm and a vertical incision along both sides of the chest opens the chest cavity. The right atrium of the heart is cut, and a needle is inserted into the left ventricle (47,50).

It is recommended to perform the cardiac perfusion on a surgical tray or similar platform to contain the exsanguinated blood. Confirm that the mouse is at an appropriate plane of anesthesia using toe and/or tail pinches. Next, open the chest cavity by performing a horizontal incision beneath the rib cage and a vertical incision along both sides of the chest (see Fig 3C) (47). Use hemostats to assist with holding the chest open to access the heart. Then, perform a small incision on the right atrium of the heart to allow blood to exit the body. This is followed by inserting a butterfly needle into the left ventricle of the heart. Use a syringe pump to perfuse 10

mL of saline into the heart at a rate of 2 mL/min. Afterwards, perfuse 10 mL of formalin at a rate of 2 mL/min.

Brain extraction

Remove the head by cutting caudal of the skull with scissors (bone scissors or large scissors preferred). Cut the scalp to create two folds and expose the cranium. Using angled microscissors, gently cut upwards from the foramen magnum to approximately the location of bregma on the brain. Using a set of scissors, perform a lateral cut directly rostral to the olfactory bulbs. This cut should split the remainder of the skull down the centerline beyond bregma. Use fine tweezers or a spatula to pry open each hemisphere of the skull. Gently separate the brain from the base of the skull with a spatula. Sever any nerves connecting the brain to the skull. Place the brain in ~10 mL of 10% formalin to completely submerge the brain. After 24h, store the brain in PBS with 0.02% sodium azide at 4°C until further tissue processing.

(Optional) Exogenous labeling of hemosiderin with Prussian blue for cerebral microhemorrhage visualization

The following procedures are based on 1-mm thick coronal sections of a bisected brain. Volumes and times may need to be adjusted for tissues of different sizes.

Prepare a working solution of 10% w/v of potassium ferrocyanide (10 g of potassium ferrocyanide per 100 mL of DIW). Use a magnetic stir plate to mix the solution for at least 20 minutes. Next, prepare a working solution of hydrochloric acid that is 20% of stock hydrochloric acid. Mix the solutions of potassium ferrocyanide and hydrochloric acid in a 1:1 ratio. Approximately 5 mL of the mixed solution is used per sample. This solution should be prepared prior to each staining session.

Wash samples in 5 mL of DIW with shaking. Submerge each sample into 5 mL of the

working potassium ferrocyanide/hydrochloric acid solution for 1 hour. Afterward, perform a final DIW wash for 5 minutes. Store the samples in PBS with 0.02% sodium azide at 4 C°.

Tissue clearing

The following procedure is modified from the established iDISCO protocols (4). Wash durations were modified for 1-mm thick coronal sections of a bisected brain.

Perform a series of methanol washes (20%, 40%, 60%, 80%, 100%, and 100%, balance DIW) each for 20 minutes with shaking. Microcentrifuge tubes of 1.5 mL (or larger for larger samples) are recommended. Fill the tubes fully to minimize exposure to oxygen. Next, incubate the samples in a solution of 66% dichloromethane and 33% methanol for one hour with shaking. The sample may be stored overnight in this situation if desired, without shaking. Next, incubate the sample in dichloromethane twice for 15 minutes with shaking. Lastly, store the samples in dibenzyl ether at 4°C until imaging.

Imaging with confocal microscopy

When imaging samples that have been cleared following the iDISCO protocol, it is recommended to image the sample while submerged in dibenzyl ether. There are various methods to safely house a sample with dibenzyl ether and protect the imaging objective. A straightforward method is to create an epoxy well on a cover glass to surround the sample and hold the dibenzyl ether.

To image the vasculature labeled with the lectin-DyLight-649, use an appropriate wavelength (633 nm can work) with an emission band of approximately 650-750 nm. To visualize microhemorrhages labeled with Prussian blue, locate regions of Prussian blue positivity using a white light source. Simultaneously collect a fluorescent image of the vasculature and a transmittance image to co-register the vascular fluorescence with cerebral

microhemorrhages. This workflow along with representative images are depicted in Fig 4.

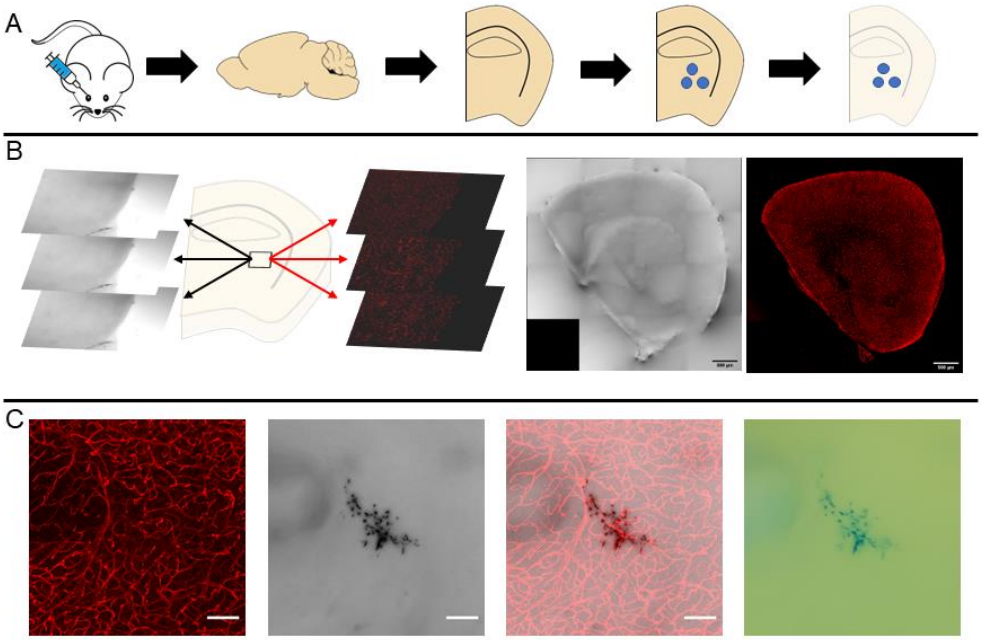

Fig 4. Workflow for 3D visualization of cerebral microvasculature cerebral microhemorrhage in thick tissue sections. A) Vasculature is labeled via retroorbital injection of lectin-DyLight-649. Brains are then sectioned, stained, and cleared. B) Depiction of z-stack imaging and tile stitching for a fluorescence channel and a transmission channel via confocal microscopy. C) From left to right: fluorescent image of microvascular network in a 70 µm thick tissue region, transmission image of cerebral microhemorrhage in the same tissue region, overlayed image of both imaging channels, eyepiece view of Prussian blue positive cerebral microhemorrhage. Scale bars are 100 µm.

In addition to imaging brain microvasculature, the combination of iDISCO and lectin-DyLight-649 enables visualization of the microvascular network of other organs. Light-sheet microscopy can be used as an alternative to confocal microscopy to rapidly generate 3D reconstructions of the vascular network with minimal photobleaching. Fig 5 shows representative images of different labeled and cleared organs imaged with confocal microscopy and light-sheet microscopy.

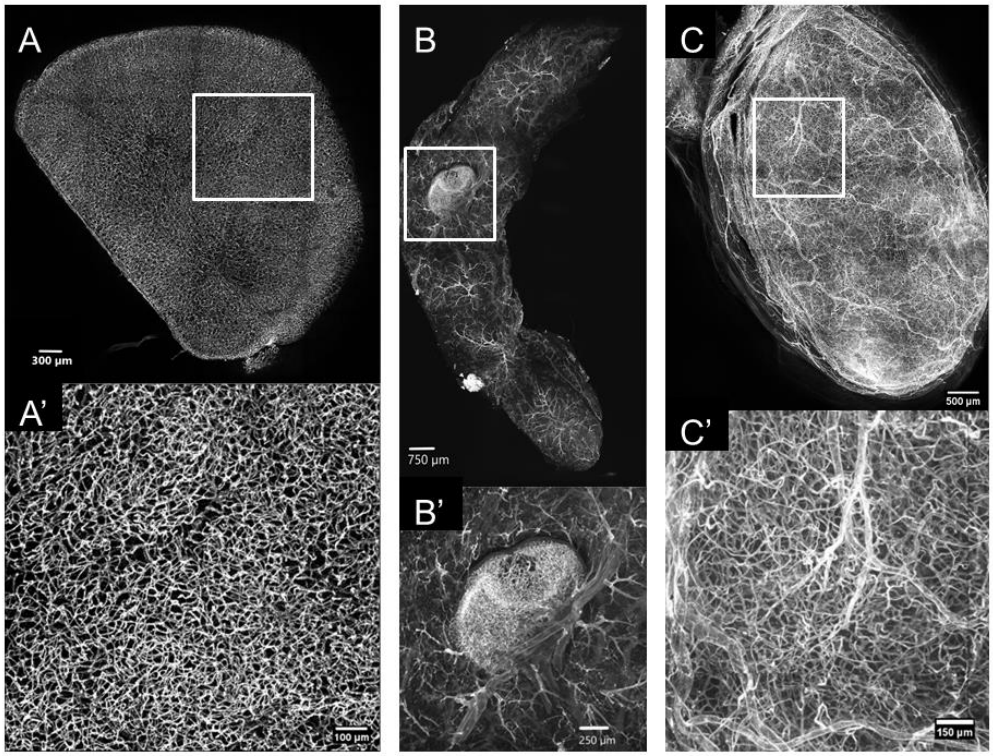

Fig 5. Lectin-DyLight-649 labeling and iDISCO optical clearing enable detailed visualization of mouse organ microvasculature. A) Confocal image of a 1-mm thick coronal hemisection of the brain. A') Magnified view of A. B) Light-sheet image of a mammary gland with a lymph node. B') Magnified view of B. C) Light-sheet image of a bladder. C') Magnified view of C.

Vascular segmentation

There are various segmentation methods to isolate the fluorescent vasculature from the image background. The iterative selection thresholding method was implemented to binarize the fluorescent images (Fig 6) (51). This algorithm was selected due to its simplicity and objectivity and was performed using custom-written code in MATLAB. Vessel parameters such as vascular density and tortuosity can be calculated from the resulting segmented images. An open-source neuron tracing software known as neuTube was used to quantify vessel sizes.

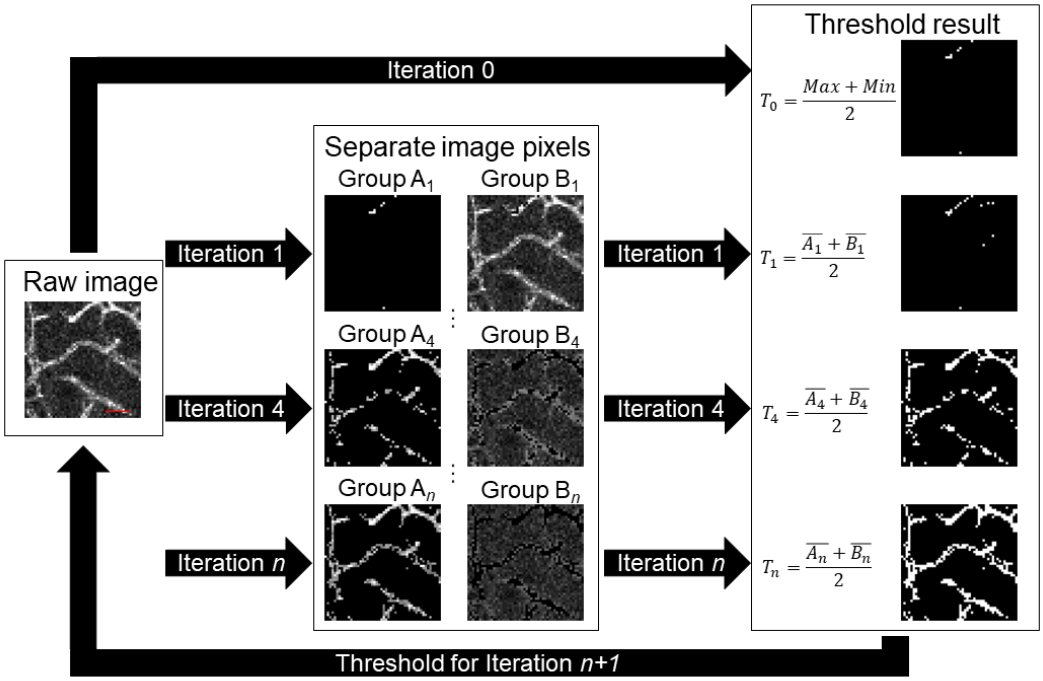

Fig 6. Schematic of iterative selection thresholding method for images of fluorescent vasculature. An initial threshold is selected as the average of the maximum and minimum voxel intensities present in the image. The subsequent iteration assigns voxels to group A_n if a voxel has an intensity greater than the threshold of the previous iteration, or to group B_n if a voxel has an intensity less than the threshold of the previous threshold. Next, the average intensity within each group is calculated, and the average of those two values determines the new threshold. This process is repeated until the change in threshold is less than one intensity value. Scale bar is 25 µm.

Using MATLAB, a 3x3x1 median filter removes noise within the image data. The iterative selection threshold method is applied by selecting an initial threshold value, T_0. The initial value is the average value of the maximum intensity and the minimum intensity of all voxels of an image.

$$T_0 = \frac{Max + Min}{2} \quad (1)$$

All voxels within an image are separated into two groups: group A_n if a voxel has an intensity

equal to or greater than the threshold value of the previous iteration, or group B_n if a voxel has an intensity below the threshold value of the previous iteration.

$$A_n \geq T_n, B_n < T_n \quad (2)$$

The threshold value of the subsequent iteration is calculated as the average value of the average intensity within groups A_n and B_n.

$$T_n = \frac{\overline{A_n} + \overline{B_n}}{2} \quad (3)$$

This threshold value is compared to the threshold value of the previous iteration. If the difference between the two values is less than 1, the procedure is complete, and the current threshold value is selected. If the difference between the two values is greater than or equal to 1, the procedure repeats for another iteration.

$$If\ |T_n - T_{n-1}| < 1, then\ stop \quad (4)$$

Optional morphological operations can be applied to the resulting binarized image to adjust segmentation results further. The exact parameters for these steps will vary with image acquisition parameters (particularly resolution).

For example, size filtering is performed by removing objects with a volume less than ~50 μm^3 (the exact voxel size will vary based on image resolution) based on an 18-point connectivity scheme. Morphological closing using a spherical structural element with a radius of 1 is applied to close gaps throughout the image. Vascular density can be quantified through built-in MATLAB functions to generate a skeletonized structure, a single-pixel width line along the

centerline of vessels, of the vascular image (21). From there, density can be calculated by dividing the total length of the skeleton by a given area. Vessel tortuosity can be calculated by dividing the shortest distance between two endpoints of a vessel and the total length of the vessel (52). A complete vessel is defined as the length of the vessel between two branch points.

neuTube tracing to quantify vessel diameters

neuTube is an open-source neuron tracing software that can be applied to tracing tubular structures, such as vasculature (46). Automated tracing can be performed on binarized vasculature images in TIF file format. neuTube will output information in an SWC format where tubular structures are simplified into individual nodes with x, y, z coordinates, a radius, and node connectivity information. Each node will be a ‘parent’ to an adjacent ‘child’ node which provides the necessary information to understand how these nodes are connected in space.

Nodal connectivity is used to identify individual vessels based on specific rules. Nodes are defined as branch nodes if they serve as the parent of two different nodes. A node is defined as an end node if it lacks a child node. Individual vessels are defined as a series of nodes bordered by two branch nodes or one branch node and an end node, including the nodes at the borders. The diameter of an individual vessel is defined as the average diameter of all nodes that make up an individual vessel.

Anticipated results

The procedures detailed herein present a simple method for producing optically-cleared (>1-mm thick) tissue samples with fluorescently labeled vasculature. Samples can then be imaged to generate 3D images of the microvasculature. Our presented results are primarily from brain samples, but the procedures can be easily translated to other organs. The described segmentation method using custom MATLAB scripts and neuTube presents an automated

method to convert the fluorescent images into binary images. The binary images can then be used to characterize microvasculature by quantifying vessel density and vessel sizes. The procedures here can be enhanced by using additional histology dyes or immunohistochemistry to label biomarkers or other structures of interest in tissue. In doing so, one can visualize and quantify the microvasculature surrounding these biomarkers to gain insight into their relationship to each other.

Validation

Segmentation results

Manually segmented images were used as a ground truth comparison of automated segmented images. Images from various brain sections across three different animals were used. Each section was imaged by collecting a stack of images that spans the entire thickness of the section. Automated segmentation was performed on each image stack. In addition, manual segmentation was performed on 50 randomly generated ROIs across all images. Each ROI was presented as a maximum intensity projection (MIP) image of a 50x50x5 voxel (113x113x38 µm) region. A MIP is used to present a 2D image that is more feasible for tracing. One author [DFX] was tasked with using MATLAB to outline every object within the image that the author determined to belong to a vessel. The corresponding 50x50x5 voxel region MIP from the automated segmented image was compared. Four representative examples of this are depicted in Fig 7. Across the 50 ROIs, the average sensitivity was 80±8%, and the average specificity was 90±5%. The Dice similarity coefficient between manually segmented and automated segmented images was calculated across all ROIs. This coefficient can measure similarity between two sets of Boolean data and ranges between 0 and 1, where 1 represents identical data, and 0 represents opposite data (53). The average Dice similarity coefficient across 50 ROIs was 0.71±0.07.

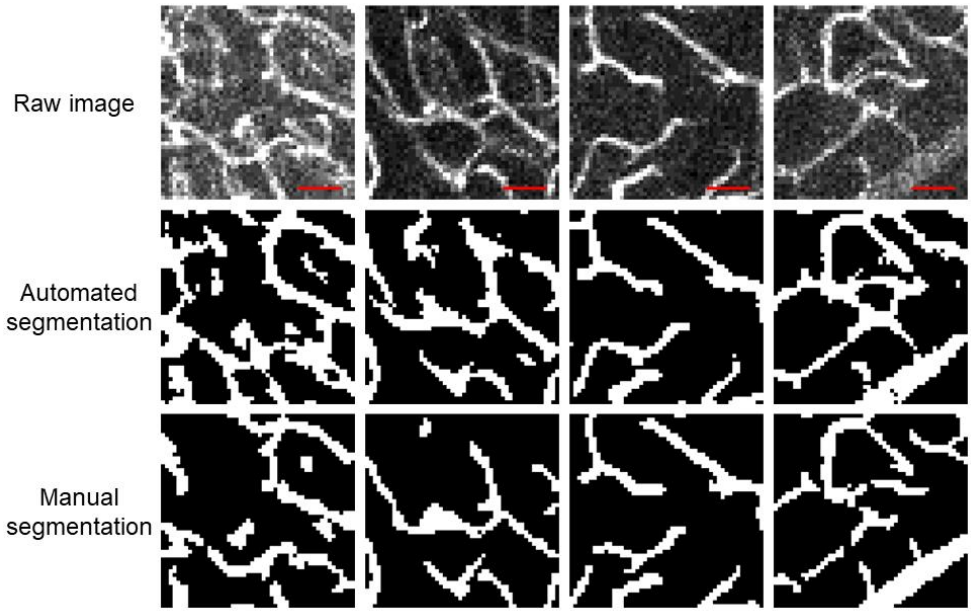

Fig 7. Manual and automated segmentation results. Four examples of different 50x50 pixel regions are shown. Scale bar is 25 µm.

Diameter results with neuTube

Manually measured diameters of individual vessels were used as a ground truth comparison for neuTube approximated vessel diameters. Images from various brain sections across three different animals were used. One author (DFX) was presented with a randomly generated 50x50x5 voxel (113x113x38 µm) size region as a MIP. Within the image, the user was tasked with using MATLAB to estimate the diameter of a single vessel in the image at five different points along the vessel by drawing lines approximately perpendicular to the centerline of the vessel. In neuTube, five nodes along the corresponding vessel were selected. The average of the five manual diameter measurements via MATLAB and the five automated diameter measurements via neuTube were compared. Two representative examples of this are depicted in Fig 8. The absolute difference between diameter measurements was 1.16±0.73 µm (n=50 vessels of diameters ranging from 1.78 µm to 3.19 µm).

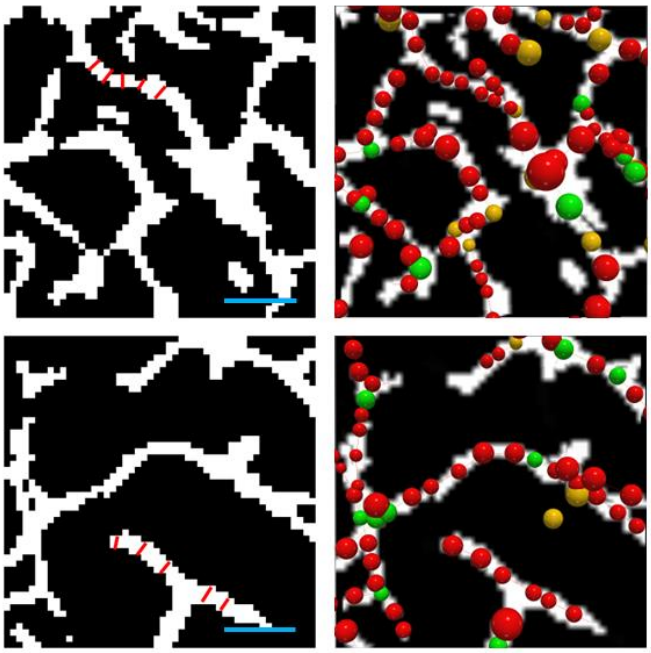

Fig 8. Manual and neuTube diameter results. Two different 50x50 pixel regions are shown, where one vessel is selected for manual measurement. Scale bar is 25 μm.

Potential applications

As angiogenesis occurs in organs, endothelial cells respond to local signals to adapt vessels to the surrounding environment (54). Angiogenesis plays an essential role in tumor formation. In tumors, angiogenesis directly impacts tumor growth and metastasis. Overexpression of proangiogenic factors leads to uncontrolled vascular growth in tumors (55). As a result, anti-angiogenic drugs are frequently used as a potential treatment option for cancer. Lectin-DyLight-649 combined with iDISCO presents a robust procedure for labeling the microvasculature in all areas in the body, including tumors. Changes in vessel density, tortuosity, and diameters can be quantified to evaluate the efficacy of novel anti-angiogenic treatments.

Ischemic strokes occur when there is a significant drop in cerebral blood flow due to

occlusion in a cerebral artery. A major consequence of such an event is necrosis of neurons due to deficient blood supply (56). A method to visualize the microvascular network and the surrounding neurons, astrocytes, and glial cells can provide a detailed 3D snapshot of the brain in response to an ischemic stroke and monitor potential treatments over time.

In addition to visualizing cerebral microhemorrhages within the surrounding microvascular network and providing improved capability to estimate size range of these lesions, our approach can provide enhanced imaging for other disease entities. For example, a growing body of literature suggests a contribution of dysfunctional regulation of cerebral blood flow and various types of cognitive impairment (3). The ability to visualize the cerebral microvasculature in three dimensions offers a new gateway potentially leading to the identification of novel treatment targets for neurological disorders.

Disclosures

The authors do not have any competing interests to disclose.

Acknowledgements

This work was supported in part by the Arnold and Mabel Beckman Foundation and the National Institutes of Health (Nos. R21AG066000, 5TL1TR001415-07, P41EB015890, R01NS020989, and R21NS111984). This study was made possible in part through access to the Optical Biology Core Facility of the Developmental Biology Center, a shared resource supported by the Cancer Center Support Grant (CA-62203) and Center for Complex Biological Systems Support Grant (GM-076516) at the University of California, Irvine

REFERENCES

1. Carmeliet P, Jain RK. Molecular mechanisms and clinical applications of angiogenesis. Nature. 2011 May 18;473(7347):298–307. Available from: 10.1038/nature10144
2. Haller S, Vernooij MW, Kuijer JPA, Larsson EM, Jäger HR, Barkhof F. Cerebral Microbleeds: Imaging and Clinical Significance. Radiology. 2018 Apr;287(1):11–28. Available from: 10.1148/radiol.2018170803
3. Sweeney MD, Kisler K, Montagne A, Toga AW, Zlokovic B V. The role of brain vasculature in neurodegenerative disorders. Nat Neurosci. 2018;21(10):1318–31. Available from: 10.1038/s41593-018-0234-x
4. Renier N, Wu Z, Simon DJ, Yang J, Ariel P, Tessier-Lavigne M. IDISCO: A simple, rapid method to immunolabel large tissue samples for volume imaging. Cell. 2014;159(4):896–910. Available from: 10.1016/j.cell.2014.10.010
5. Susaki EA, Tainaka K, Perrin D, Kishino F, Tawara T, Watanabe TM, et al. Whole-brain imaging with single-cell resolution using chemical cocktails and computational analysis. Cell. 2014;157(3):726–39. Available from: 10.1016/j.cell.2014.03.042
6. Chung K, Wallace J, Kim SY, Kalyanasundaram S, Andalman AS, Davidson TJ, et al. Structural and molecular interrogation of intact biological systems. Nature. 2013 May 16;497(7449):332–7. Available from: 10.1038/nature12107
7. Kalaria RN, Akinyemi R, Ihara M. Stroke injury, cognitive impairment and vascular dementia. Biochim Biophys Acta - Mol Basis Dis. 2016 May;1862(5):915–25. Available from: 10.1016/j.bbadis.2016.01.015
8. Moy AJ, Lo PC, Choi B. High-resolution visualization of mouse cardiac microvasculature using optical histology. Biomed Opt Express. 2014 Jan 1;5(1):69. Available from: 10.1364/BOE.5.000069
9. Kirst C, Skriabine S, Vieites-Prado A, Topilko T, Bertin P, Gerschenfeld G, et al. Mapping

the Fine-Scale Organization and Plasticity of the Brain Vasculature. Cell. 2020;180(4):780-795.e25. Available from: 10.1016/j.cell.2020.01.028

10. Khouri K, Xie DF, Crouzet C, Bahani AW, Cribbs DH, Fisher MJ, et al. Simple methodology to visualize whole-brain microvasculature in three dimensions. Neurophotonics. 2021 Apr 19;8(02):1–10. Available from: 10.1117/1.NPh.8.2.025004

11. Crouzet C, Jeong G, Chae RH, LoPresti KT, Dunn CE, Xie DF, et al. Spectroscopic and deep learning-based approaches to identify and quantify cerebral microhemorrhages. Sci Rep. 2021 Dec 21;11(1):10725. Available from: 10.1038/s41598-021-88236-1

12. Lo P, Crouzet C, Vasilevko V, Choi B. Visualization of microbleeds with optical histology in mouse model of cerebral amyloid angiopathy. Microvasc Res. 2016;105:109–13. Available from: 10.1016/j.mvr.2016.02.002

13. Sumbria RK, Grigoryan MM, Vasilevko V, Paganini-Hill A, Kilday K, Kim R, et al. Aging exacerbates development of cerebral microbleeds in a mouse model. J Neuroinflammation. 2018 Dec 6;15(1):69. Available from: 10.1186/s12974-018-1092-x

14. Zhu J, Yu T, Li Y, Xu J, Qi Y, Yao Y, et al. MACS: Rapid Aqueous Clearing System for 3D Mapping of Intact Organs. Adv Sci. 2020 Apr 25;7(8):1903185. Available from: 10.1002/advs.201903185

15. Hama H, Hioki H, Namiki K, Hoshida T, Kurokawa H, Ishidate F, et al. ScaleS: an optical clearing palette for biological imaging. Nat Neurosci. 2015 Oct 14;18(10):1518–29. Available from: 10.1038/nn.4107

16. Nehrhoff I, Ripoll J, Samaniego R, Desco M, Gómez-Gaviro MV. Looking inside the heart: a see-through view of the vascular tree. Biomed Opt Express. 2017 Jun 1;8(6):3110. Available from: 10.1364/BOE.8.003110

17. Nishimura W, Sakaue-Sawano A, Takahashi S, Miyawaki A, Yasuda K, Noda Y. Optical clearing of the pancreas for visualization of mature β-cells and vessels in mice. Islets. 2018 May 4;10(3):e1451282. Available from: 10.1080/19382014.2018.1451282

18. Fu YY, Tang SC. Optical clearing facilitates integrated 3D visualization of mouse ileal microstructure and vascular network with high definition. Microvasc Res. 2010;80(3):512–21. Available from: 10.1016/j.mvr.2010.06.003

19. Loren M, Crouzet C, Bahani A, Vasilevko V, Choi B. Optical clearing potential of immersion-based agents applied to thick mouse brain sections. Maitland KC, editor. PLoS One. 2019 May 10;14(5):e0216064. Available from: 10.1371/journal.pone.0216064

20. Qi Y, Yu T, Xu J, Wan P, Ma Y, Zhu J, et al. FDISCO: Advanced solvent-based clearing method for imaging whole organs. Sci Adv. 2019 Jan 4;5(1):1–14. Available from: 10.1126/sciadv.aau8355

21. White SM, George SC, Choi B. Automated computation of functional vascular density using laser speckle imaging in a rodent window chamber model. Microvasc Res. 2011;82(1):92–5. Available from: 10.1016/j.mvr.2011.03.006

22. Jing D, Zhang S, Luo W, Gao X, Men Y, Ma C, et al. Tissue clearing of both hard and soft tissue organs with the pegasos method. Cell Res. 2018;28(8):803–18. Available from: 10.1038/s41422-018-0049-z

23. Matryba P, Sosnowska A, Wolny A, Bozycki L, Greig A, Grzybowski J, et al. Systematic Evaluation of Chemically Distinct Tissue Optical Clearing Techniques in Murine Lymph Nodes. J Immunol. 2020 Mar 1;204(5):1395–407. Available from: 10.4049/jimmunol.1900847

24. Miyawaki T, Morikawa S, Susaki EA, Nakashima A, Takeuchi H, Yamaguchi S, et al. Visualization and molecular characterization of whole-brain vascular networks with capillary resolution. Nat Commun. 2020;11(1):1–11. Available from: 10.1038/s41467-020-14786-z

25. McKey J, Cameron LA, Lewis D, Batchvarov IS, Capel B. Combined iDISCO and CUBIC tissue clearing and lightsheet microscopy for in toto analysis of the adult mouse ovary†. Biol Reprod. 2020 Apr 24;102(5):1080–9. Available from: 10.1093/biolre/ioaa012

26. Lugo-Hernandez E, Squire A, Hagemann N, Brenzel A, Sardari M, Schlechter J, et al. 3D visualization and quantification of microvessels in the whole ischemic mouse brain using solvent-based clearing and light sheet microscopy. J Cereb Blood Flow Metab. 2017 Oct 28;37(10):3355–67. Available from: 10.1177/0271678X17698970

27. Zhu D, Wang J, Zhi Z, Wen X, Luo Q. Imaging dermal blood flow through the intact rat skin with an optical clearing method. J Biomed Opt. 2010;15(2):026008. Available from: 10.1117/1.3369739

28. Liebmann T, Renier N, Bettayeb K, Greengard P, Tessier-Lavigne M, Flajolet M. Three-Dimensional Study of Alzheimer's Disease Hallmarks Using the iDISCO Clearing Method. Cell Rep. 2016;16(4):1138–52. Available from: 10.1016/j.celrep.2016.06.060

29. Datta A, Sarmah D, Mounica L, Kaur H, Kesharwani R, Verma G, et al. Cell Death Pathways in Ischemic Stroke and Targeted Pharmacotherapy. Transl Stroke Res. 2020 Dec 26;11(6):1185–202. Available from: 10.1007/s12975-020-00806-z

30. Khoradmehr A, Mazaheri F, Anvari M, Tamadon A. A Simple Technique for Three-Dimensional Imaging and Segmentation of Brain Vasculature U sing Fast Free-of-Acrylamide Clearing Tissue in Murine. Cell J. 2019 Apr;21(1):49–56. Available from: 10.22074/cellj.2019.5684

31. Ivins S, Roberts C, Vernay B, Scambler PJ. Analysis of Coronary Vessels in Cleared Embryonic Hearts. J Vis Exp. 2016 Dec 7;2016(118):1–9. Available from: 10.3791/54800

32. Kolesová H, Čapek M, Radochová B, Janáček J, Sedmera D. Comparison of different tissue clearing methods and 3D imaging techniques for visualization of GFP-expressing mouse embryos and embryonic hearts. Histochem Cell Biol. 2016 Aug 4;146(2):141–52. Available from: 10.1007/s00418-016-1441-8

33. Cai R, Pan C, Ghasemigharagoz A, Todorov MI, Förstera B, Zhao S, et al. Panoptic imaging of transparent mice reveals whole-body neuronal projections and skull–meninges connections. Nat Neurosci. 2019;22(2):317–27. Available from: 10.1038/s41593-018-

0301-3

34. Harrison CH, Buckland GR, Brooks SE, Johnston DA, Chatelet DS, Liu AKL, et al. A novel method to visualise the three-dimensional organisation of the human cerebral cortical vasculature. J Anat. 2018 Jun;232(6):1025–30. Available from: 10.1111/joa.12805

35. Krolewski DM, Kumar V, Martin B, Tomer R, Deisseroth K, Myers RM, et al. Quantitative validation of immunofluorescence and lectin staining using reduced CLARITY acrylamide formulations. Brain Struct Funct. 2018 Mar 14;223(2):987–99. Available from: 10.1007/s00429-017-1583-z

36. Oren R, Fellus-Alyagor L, Addadi Y, Bochner F, Gutman H, Blumenreich S, et al. Whole Organ Blood and Lymphatic Vessels Imaging (WOBLI). Sci Rep. 2018;8(1):1–9. Available from: 10.1038/s41598-018-19663-w

37. Huang J, Brenna C, Khan A ul M, Daniele C, Rudolf R, Heuveline V, et al. A cationic near infrared fluorescent agent and ethyl-cinnamate tissue clearing protocol for vascular staining and imaging. Sci Rep. 2019 Dec 24;9(1):521. Available from: 10.1038/s41598-018-36741-1

38. Carrillo M, Chuecos M, Gandhi K, Bednov A, Moore DL, Maher J, et al. Optical tissue clearing in combination with perfusion and immunofluorescence for placental vascular imaging. Medicine (Baltimore). 2018 Sep;97(39):e12392. Available from: 10.1097/MD.0000000000012392

39. Lagerweij T, Dusoswa SA, Negrean A, Hendrikx EML, de Vries HE, Kole J, et al. Optical clearing and fluorescence deep-tissue imaging for 3D quantitative analysis of the brain tumor microenvironment. Angiogenesis. 2017 Nov 11;20(4):533–46. Available from: 10.1007/s10456-017-9565-6

40. Yi Y, Men Y, Jing D, Luo W, Zhang S, Feng JQ, et al. 3-dimensional visualization of implant-tissue interface with the polyethylene glycol associated solvent system tissue

clearing method. Cell Prolif. 2019 May 3;52(3):e12578. Available from: 10.1111/cpr.12578

41. Singh JN, Nowlin TM, Seedorf GJ, Abman SH, Shepherd DP. Quantifying three-dimensional rodent retina vascular development using optical tissue clearing and light-sheet microscopy. J Biomed Opt. 2017 Jul 18;22(07):1. Available from: 10.1117/1.JBO.22.7.076011

42. Li Y, Song Y, Zhao L, Gaidosh G, Laties AM, Wen R. Direct labeling and visualization of blood vessels with lipophilic carbocyanine dye DiI. Nat Protoc. 2008 Nov 9;3(11):1703–8. Available from: 10.1038/nprot.2008.172

43. Peviani M, Spano G, Pagani A, Brugnara G, Covino C, Galli R, et al. Lipophilic dye-compatible brain clearing technique allowing correlative magnetic resonance/high-resolution fluorescence imaging in rat models of glioblastoma. Sci Rep. 2020;10(1):1–15. Available from: 10.1038/s41598-020-75137-y

44. Moy AJ, Capulong B V., Saager RB, Wiersma MP, Lo PC, Durkin AJ, et al. Optical properties of mouse brain tissue after optical clearing with FocusClear™. J Biomed Opt. 2015 Sep 21;20(9):095010. Available from: 10.1117/1.JBO.20.9.095010

45. Moy AJ, Wiersma MP, Choi B. Optical Histology: A Method to Visualize Microvasculature in Thick Tissue Sections of Mouse Brain. Georgakoudi I, editor. PLoS One. 2013 Jan 23;8(1):e53753. Available from: 10.1371/journal.pone.0053753

46. Feng L, Zhao T, Kim J. neuTube 1.0: A New Design for Efficient Neuron Reconstruction Software Based on the SWC Format. eneuro. 2015 Jan 29;2(1):ENEURO.0049-14.2014. Available from: 10.1523/ENEURO.0049-14.2014

47. Gage GJ, Kipke DR, Shain W. Whole Animal Perfusion Fixation for Rodents. J Vis Exp. 2012 Jul 30;(65):1–9. Available from: 10.3791/3564

48. Yardeni T, Eckhaus M, Morris HD, Huizing M, Hoogstraten-Miller S. Retro-orbital injections in mice. Lab Anim (NY). 2011 May 20;40(5):155–60. Available from:

10.1038/laban0511-155

49. Robertson RT, Levine ST, Haynes SM, Gutierrez P, Baratta JL, Tan Z, et al. Use of labeled tomato lectin for imaging vasculature structures. Histochem Cell Biol. 2015 Feb 23;143(2):225–34. Available from: 10.1007/s00418-014-1301-3

50. Prabhakar S, Lule S, da Hora CC, Breakefield XO, Cheah PS. AAV9 transduction mediated by systemic delivery of vector via retro-orbital injection in newborn, neonatal and juvenile mice. Exp Anim. 2021;70(4):20–0186. Available from: 10.1538/expanim.20-0186

51. Ridler TW, Calvard S. Picture Thresholding Using An Interactive Selection Method. IEEE Trans Syst Man Cybern [Internet]. 1978;smc-8(8):630–2.

52. Hart WE, Goldbaum M, Côté B, Kube P, Nelson MR. Measurement and classification of retinal vascular tortuosity. Int J Med Inform. 1999 Feb;53(2–3):239–52. Available from: 10.1016/S1386-5056(98)00163-4

53. Dice LR. Measures of the Amount of Ecologic Association Between Species. Ecology [Internet]. 1945;26(3):297–302.

54. McDonald DM. Angiogenesis and Vascular Remodeling in Inflammation and Cancer: Biology and Architecture of the Vasculature. In: Angiogenesis. Boston, MA: Springer US; 2008. p. 17–33. Available from: 10.1007/978-0-387-71518-6_2

55. Li T, Kang G, Wang T, Huang H. Tumor angiogenesis and anti-angiogenic gene therapy for cancer (Review). Oncol Lett. 2018 May 17;16(1):687–702. Available from: 10.3892/ol.2018.8733

56. Datta A, Sarmah D, Mounica L, Kaur H, Kesharwani R, Verma G, et al. Cell Death Pathways in Ischemic Stroke and Targeted Pharmacotherapy. Transl Stroke Res. 2020 Dec 26;11(6):1185–202. Available from: 10.1007/s12975-020-00806-z